Langmuir

Article

pubs.acs.org/Langmuir

Synthesis and Organic Surface Modification of Luminescent, Lanthanide-Doped Core/Shell Nanomaterials (LnF_3@SiO_2@NH_2@Organic Acid) for Potential Bioapplications: Spectroscopic, Structural, and *in Vitro* Cytotoxicity Evaluation

Marcin Runowski,[†] Anna Ekner-Grzyb,*[,‡] Lucyna Mrówczyńska,[§] Sangeetha Balabhadra,[†] Tomasz Grzyb,[†] Jan Paczesny,[∥] Anna Zep,[⊥] and Stefan Lis*[,†]

[†]Department of Rare Earths, Faculty of Chemistry, Adam Mickiewicz University, Grunwaldzka 6, 60-780 Poznań, Poland

[‡]Department of Behavioural Ecology, Faculty of Biology, Adam Mickiewicz University, Umultowska 89, 61-614 Poznań, Poland

[§]Department of Cell Biology, Faculty of Biology, Adam Mickiewicz University, Umultowska 89, 61-614 Poznań, Poland

[∥]Department of Soft Condensed Matter and Fluids, Institute of Physical Chemistry of the Polish Academy of Sciences, Kasprzaka 44/52, 01-224 Warsaw, Poland

[⊥]Laboratory of Physicochemistry of Dielectrics and Magnetics, Faculty of Chemistry, University of Warsaw, Żwirki i Wigury 101, 02-089 Warsaw, Poland

Supporting Information

ABSTRACT: A facile coprecipitation reaction between Ce^{3+}, Gd^{3+}, Tb^{3+}, and F^- ions, in the presence of glycerine as a capping agent, led to the formation of ultrafine, nanocrystalline CeF_3:Tb^{3+} 5%, Gd^{3+} 5% (LnF_3). The as-prepared fluoride nanoparticles were successfully coated with an amine modified silica shell. Subsequently, the obtained LnF_3@SiO_2@NH_2 nanostructures were conjugated with 4-ethoxybenzoic acid in order to prove the possibility of organic modification and obtain a new functional nanomaterial. All of the nanophosphors synthesized exhibited intense green luminescence under UV light irradiation. Based on TEM (transmission electron microscopy) measurements, the diameters of the cores (≈12 nm) and core/shell particles (≈50 nm) were determined. To evaluate the cytotoxic activity of the nanomaterials obtained, their effect on human erythrocytes was investigated. LnF_3 nanoparticles were bound to the erythrocyte membrane, without inducing any cytotoxic effects. After coating with silica, the nanoparticles revealed significant cytotoxicity. However, further functionalization of the nanomaterial with $-NH_2$ groups as well as conjugation with 4-ethoxybenzoic acid entailed a decrease in cytotoxicity of the core/shell nanoparticles.

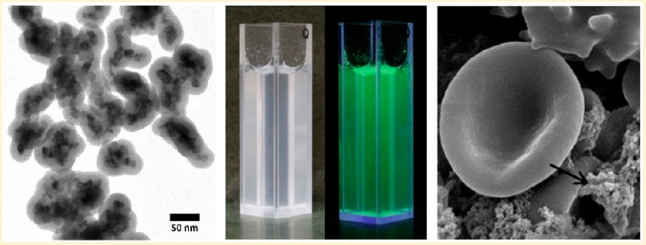

1. INTRODUCTION

Nanoscience and nanotechnology are broad and interdisciplinary areas of research that have been growing explosively worldwide in the past years.[1−3] Nanoparticles (NPs) have large surface area to volume ratios, which causes changes in their optoelectronic, magnetic, and catalytic properties in comparison to their bulk counterparts.[3−5] Because of their nanometric size, which is much smaller than living cells, they are suitable for numerous bioapplications. They can form stable aqueous colloids, which are useful for bioimaging.[1,2]

Nowadays, luminescent nanomaterials doped with lanthanide ions (Ln^{3+}) have attracted considerable attention as a result of their potential applications in various areas, such as field-effect transistors (FET), optoelectronics, optical storage, solar cells, and color displays.[6,7] Moreover, their unique properties allow for applications in biorelated areas, as biomedical markers *in vitro* and *in vivo*, in bioimaging, cancer therapy, or drug delivery.[6,8] The alternative particles, such as organic dyes and semiconductor quantum dots (QDs), have also been employed as phosphor materials in industry and luminescent markers in biology.[1,3] However, both of them have some limitations. Organic dyes often exhibit rapid photobleaching, and QDs can be cytotoxic, which limit their *in vivo* applications.[9] Hence, Ln^{3+}-doped nanophosphors are promising and novel nanomaterials due to their excellent properties such as narrow emission lines, long radiative lifetimes, large Stokes shifts, high quantum yields of luminescence, nonphotobleaching, and low toxicity.[2,7,8] However, Ln^{3+} ions have relatively low absorption coefficients, in comparison to organic dyes and QDs, which makes it necessary to use energy transfer (ET) phenomenon in lanthanide-doped NPs. This process can effectively increase the luminescence efficiency and allows for the possibility of designing the system for sensitivity to selected spectral regions; e.g., Yb^{3+} or Ce^{3+} ions are sensitizers for near-infrared or UV

Received: March 25, 2014
Revised: July 16, 2014
Published: July 18, 2014

radiation, respectively.[10,11] In particular, the Ce^{3+}/Tb^{3+} ion couple has been utilized in a number of traditional phosphors for the generation of green light.[11,12] Hence, numerous dispersible NPs doped with Ce^{3+} and Tb^{3+} ions have been synthesized through a variety of techniques.[12,13] Additionally, Gd^{3+} ion decreases the energy gap between the lowest excited states of Ce^{3+} and Tb^{3+} ions which facilitates ET to Tb^{3+} ions and enhances the luminescence intensity of the system.[14]

For optical applications rare earth fluoride (REF_3) host matrices are very attractive because of their low vibrational energy (<400 cm^{-1}).[15] Because of this feature, phosphors based on REF_3 exhibit high quantum efficiencies of luminescence and low nonradiative relaxation of their electronic excited states.[16] Nowadays, several REF_3 are used or are being tested for use in such fields as optoelectronics, medicine, and industry as luminescent fibers, amplifiers, lasers, various biomaterials, etc.[17−19]

Core/shell type nanoparticles are a special kind of nanomaterial, in which the core containing the desired functional nanoparticles is covered with a nanometric shell, e.g., silica or titania.[20,21] Therefore, such hybrid nanomaterials can be multifunctional, as they reveal simultaneously the properties of the core and the shell. The core usually consists of an inorganic phase, which can exhibit the desired properties, dependent on its further applications. The formed silica shell allows for its further surface modification, simultaneously protecting the core from the environment (oxidation, aggressive agents).[22]

A simple approach is to coat the given NPs with an external silica shell.[23] Silica is stable under acidic conditions and inert against redox reactions as compared with many organic coating materials. That is why such NPs coated with silica reveal high stability of colloids in water and biological systems, resistance to aggressive agents, and radiation as well as large surface area, which is beneficial in drug delivery systems and fluorescence labeling.[24] Additionally, the silica coating provides an abundance of surface active silanol groups, which can easily undergo further functionalization and improve the ability for bioconjugation of various functional groups to such NPs.[25]

However, nanomaterials containing silica can be cytotoxic.[26−29] The toxicity of such nanostructures depends on their phase composition, size, porosity, hydrophilicity, and surface charge.[27,30,31] The mechanism of their cytotoxicity is related to the abnormal expression of oxidative stress-associated molecules. Exposure to SiO_2 may decrease a cell's viability and proliferation, induce apoptosis and protein expression, as well as change mitochondrial activity, and induce hemolysis.[27,28,32]

Amine-functionalized silica nanoparticles have been studied to achieve a reactive and biocompatible modified surface by the formation of covalent bonds and electrostatic interactions between the interfacial amino groups and other organic coupling agents, working as receptors for biomolecules.[26,33]

It is an essential issue to evaluate cytotoxicity properties of potentially biocompatible nanostructures, before their application in biology or medicine. Nanoparticles may impair a cell's function, e.g., by cell membrane integrity disruption, interference with organelle function, or disruption of the cytoskeleton. They may cause oxidative stress, apoptosis, or epigenetic effect as well.[28,34,35] Moreover, nanoparticles can adsorb biomolecules, creating a "corona" of biomolecules on their surface, which may affect biological systems.[36] Despite all these potential dangers, only a few studies dealing with the cytotoxicity of Ln^{3+}-doped nanocrystals have been conducted. Cell viability depends on the dosage, exposure time, and size of studied nanoparticles as well as on the particles' crystallinity and the presence of ligands in a given system.[27,37] The increased use of nanomaterials in many areas of life and the confirmed cytotoxic properties of many of them implies the necessity of such research.

Erythrocytes are the dominant cells (99%) in human blood, and therefore they are the most convenient systems for the study of cytotoxicity activity of new chemical compounds. Red blood cells treated with nanostructures may aggregate and potentially create a thrombus.[38] Moreover, nanoparticles can bind to the erythrocyte membrane and induce changes in its molecular structure, resulting in cell shape alterations and hemolysis.[32,39,40] However, to the best of our knowledge, there is no study on the influence of nanocrystals doped with lanthanide ions on red blood cells.

In this study, we present a synthesis and photophysical characterization of multifunctional, luminescent core/shell type nanomaterials forming stable aqueous colloids and being easily functionalized. To better understand the biological features of the nanoparticles synthesized, the impact of bare nanocrystals and surface modified core/shell type nanostructures on human erythrocytes was investigated. Our intention was to synthesize efficient and monodispersive core/shell type nanophosphors and to modify their surfaces. We wanted to obtain noncytotoxic nanomaterial, which could be further applied as contrast agents, biomarkers or simple model materials for drug delivery, tracing techniques, selective detection, etc. CeF_3 nanoparticles doped with Gd^{3+} and Tb^{3+} ions were selected as an excellent luminescent system because of its tendency to crystallize as fine nanocrystals, which can form stable aqueous colloids, exhibiting very intense green emission. The last feature is especially important in potential bioimaging applications since to opens the possibility of eliminating short-lived background radiation. The formation of core/shell NPs was achieved using lanthanide fluoride as an inorganic luminescent core, and subsequent formation of an amine functionalized silica shell, via a modified Stöber method.[41] The amine-terminated NPs were further functionalized with 4-ethoxybenzoic acid, as an exemplary reactive organic compound, which can be used for further modifications. The performed surface modifications altered the biological features of the nanomaterials synthesized, especially their cytotoxicity and the possibility of selective binding to the desired organic structures.

2. EXPERIMENTAL SECTION

2.1. Materials. Tb_4O_7 and Gd_2O_3 (Stanford Materials, 99.99%) were dissolved in a concentrated, ultrapure nitric acid, HNO_3 (POCh S.A., 67%) to prepare $Tb(NO_3)_3$ and $Gd(NO_3)_3$ aqueous solutions. $CeCl_3{\cdot}7H_2O$ (99.9%) was purchased from Sigma-Aldrich. Ammonium fluoride, NH_4F (POCh S.A., ACS grade, 98%), was used as a source of fluoride ions. Tetraethyl orthosilicate, TEOS, and 3-aminopropyltriethoxysilane, APTES (Sigma-Aldrich, reagent grade, ≥98%), were used as a source of silica and amino groups, respectively. An aqueous solution of concentrated ammonium hydroxide (Chempur, pure p.a., 25%) was used to increase the pH during the hydrolysis of silanes. 4-Ethoxybenzoyl chloride (synthetic process described in the Supporting Information) was used as a surface modifier. Glycerin, ethanol, toluene, and THF (tetrahydrofuran) were purchased from POCh S.A. (pure p.a.). Glutaraldehyde and osmium tetroxide (OsO_4) were purchased from Sigma-Aldrich. Double distilled water was used for all syntheses.

2.2. Synthesis of Luminescent Core—CeF_3:Tb^{3+} 5%, Gd^{3+} 5%. The luminescent nanoparticles were synthesized via a well-known coprecipitation method.[2,11] The synthesis was performed to obtain 1 g

dx.doi.org/10.1021/la501107a | Langmuir 2014, 30, 9533−9543

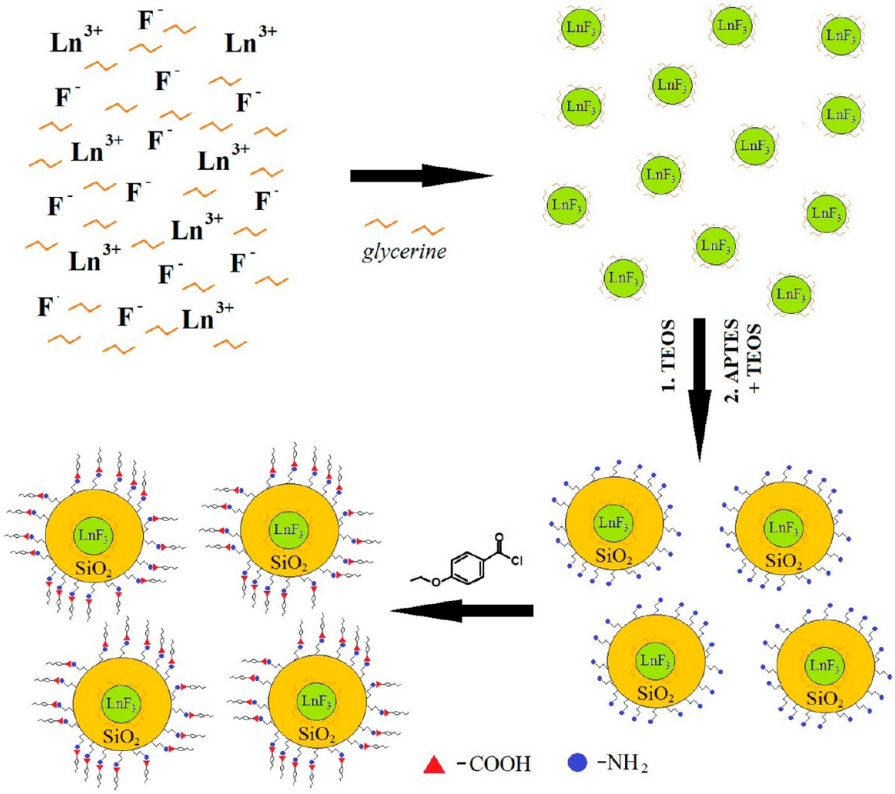

Figure 1. Synthesis scheme of CeF_3:Tb^{3+} 5%, Gd^{3+} 5%@SiO_2@NH_2@4-ethoxybenzoic acid core/shell type nanoparticles.

of the product. In order to synthesize the CeF_3:Tb^{3+} 5%, Gd^{3+} 5% nanomaterials, the solution A was prepared as follows: aqueous solutions of $Tb(NO_3)_3$, $Gd(NO_3)_3$, and $CeCl_3$ were mixed in molar ratio 5:5:90, respectively. The obtained solution containing rare earth ions was diluted with water up to 80 mL and subsequently mixed with 20 mL of glycerin (antiagglomerating agent). Subsequently solution B containing a fluoride ions source was prepared as follows: NH_4F (20% excess) was dissolved in 80 mL of water and subsequently mixed with 20 mL of glycerin. To the continuously stirred solution B, the solution A was added dropwise (the process of addition lasted approximately 20 min). After this time the reaction was finished, and a white precipitate of CeF_3:Tb^{3+} 5%, Gd^{3+} 5% was obtained. The precipitate was purified by centrifugation and washed several times with water. The product exhibited bright, green luminescence under UV lamp irradiation (λ_{ex} = 254 nm). The as-prepared product was dispersed in 50 mL of water using ultrasonication, forming a stable, homogeneous colloid.

2.3. Synthesis of Amine Modified Core/Shell Type—CeF_3:Tb^{3+} 5%, Gd^{3+} 5%@SiO_2@NH_2. A portion of 100 mg of colloidal CeF_3:Tb^{3+} 5%, Gd^{3+} 5% was transferred into a beaker, dispersed in 30 mL of water with the use of ultrasound. After that, 160 mL of ethanol and 10 mL of concentrated ammonia (hydrolysis catalyst) were added to the aqueous colloid obtained. The colloid was ultrasonicated again and then continuously stirred at ambient conditions. Subsequently, 0.25 mL of TEOS was added to the colloidal solution. After 30 min, 0.25 mL of TEOS and 0.25 mL of APTES were added to the solution. The whole process lasted 2.5 h. When the reaction was completed, the product was purified by centrifugation and washed several times with water and ethanol. The final amine modified core/shell type product exhibited bright, green luminescence under UV lamp irradiation (λ_{ex} = 254 nm) as well.

2.4. Synthesis of Core/Shell Type—CeF_3:Tb^{3+} 5%, Gd^{3+} 5%@SiO_2. In order to compare physicochemical properties of the amine modified core/shell nanomaterial with the nonmodified core/shell nanomaterial, an additional synthesis was performed using the same method as described above, but without the addition of APTES.

2.5. Surface Modification of CeF_3:Tb^{3+} 5%, Gd^{3+} 5%@SiO_2@NH_2. To the suspension of CeF_3:Tb^{3+} 5%, Gd^{3+} 5%@SiO_2@NH_2 core/shell type nanoparticles (0.8 g) in anhydrous toluene (75 mL) at ambient conditions, redistilled and dried triethylamine was added (1.0 g, 0.010 mol). The obtained mixture was stirred at 323 K for 15 min. Afterward, a solution of 4-ethoxybenzoyl chloride (1.7 g, 0.009 mol) in 10 mL of toluene was added dropwise. The mixture was stirred at 343 K for 24 h. After that, the reaction system was cooled, and then the toluene was removed using a rotary evaporator. The crude product was washed with water (100 mL) and then collected by filtration (in order to remove the triethylamine chloride formed during the process). Afterward, the resultant product was washed with methanol to remove the residual water. Subsequently, the as-prepared product was redispersed using ultrasound in THF, centrifuged, and washed several times. Here it is worth noting that the used organic compound could be easily solubilized in THF and toluene. However, toluene has a higher boiling point than THF, which was why toluene was used in the reaction.

The scheme depicted in Figure 1 presents the formation of the core/shell type luminescent nanomaterials and their surface modification.

3. CHARACTERIZATION

Microscopy measurements were performed with the transmission electron microscope JEM 1200 EXII, operating at an accelerating voltage of 80 kV. Powder XRD patterns were recorded with a Bruker AXS D8 Advance diffractometer, using Cu Kα radiation (λ = 1.5406 Å). Using the data collected from XRD, the average grain size of the nanocrystals synthesized was estimated based on Scherrer's equation:[42]

$$D = \frac{k\lambda}{\cos\theta\sqrt{\beta^2 - \beta'^2}} \quad (1)$$

where D is grain size, k is a shape factor (0.9 for spherical particles), λ is a wavelength of radiation, θ is an angle of

dx.doi.org/10.1021/la501107a | Langmuir 2014, 30, 9533−9543

diffraction, β is a full width at half-maximum (fwhm), and β' is an instrumental effect. IR spectra were recorded using an FT-IR spectrophotometer, JASCO 4200, in the transmission mode. The excitation and emission spectra were measured using a Hitachi F-7000 spectrofluorometer, at 293 K. All spectra were appropriately corrected for the instrumental response. Luminescence decay curves were collected on a QuantaMasterTM 40 spectrophotometer equipped with an Opolette 355LD UVDM tunable laser, which had a repetition rate of 20 Hz, as the excitation source and a Hamamatsu R928 photomultiplier as the detector. The hydrodynamic diameter and zeta (ζ) potential of the obtained nanoparticles were measured using Malvern Zetasizer Nano ZS equipped with a dynamic light scattering (DLS) module (He−Ne laser 633 nm, maximum 4 mW). Before measurements each compound was dispersed in Milli-Q quality water forming diluted aqueous colloids (0.2 mg/mL). The pH value in all systems was adjusted using HCl and NaOH aqueous solutions. The elemental analysis was performed using an elementar analyzer (Vario EL III). The detailed characterization of erythrocyte preparation, cytotoxicity assays, and morphology alterations is presented in the Supporting Information.

4. RESULTS AND DISCUSSION

4.1. Structure, Morphology, and Surface Properties.

Figure 2 shows the powder XRD patterns of the materials

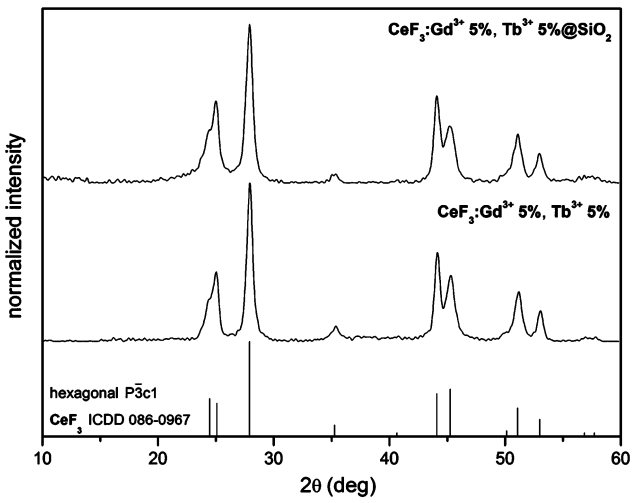

Figure 2. XRD patterns of CeF_3:Tb^{3+} 5%, Gd^{3+} 5% and CeF_3:Tb^{3+} 5%, Gd^{3+} 5%@SiO_2 nanostructures.

synthesized compared to the reference pattern from the ICDD (Inorganic Crystal Diffraction Data) database, card no. 086-0967. The CeF_3:Tb^{3+} 5%, Gd^{3+} 5% product was successfully synthesized as small, crystalline nanoparticles by coprecipitation in the presence of glycerin used as an antiagglomeration agent. The experimental diffractogram fits well to the hexagonal CeF_3 fluoride ($P\bar{3}c1$ space group). The second diffractogram recorded for the core/shell CeF_3:Tb^{3+} 5%, Gd^{3+} 5%@SiO_2 nanomaterial was similar to the pattern corresponding to the bare core because the crystalline phase in both compounds was the same. However, a slight difference could be found in the range of 20°−30° 2θ, where a small and broad reflex (overlapping with LnF_3 reflexes) assigned to the amorphous silica shell was observed (because of the partial ordering of the silica structure).[20,43] The subsequent surface modifications did not influence crystal structure of the luminescent core as well. The recorded diffractograms revealed significant reflexes broadening, which is typical of small nanoparticles. On the basis of the Scherrer equation,[42] the average grain size of the CeF_3:Tb^{3+} 5%, Gd^{3+} 5% nanocrystals synthesized was estimated as 11 ± 2 nm.

TEM images obtained for all samples are presented in Figure 3. The calculated average size of the core nanoparticles CeF_3:Tb^{3+} 5%, Gd^{3+} 5% (LnF_3) was about 12 nm (Figure 3A). The size of the LnF_3@SiO_2 nanostructures (Figure 3B) was in the range of 30−50 nm (averaged total size of the cores coated by silica shell). Larger agglomerates of the nanoparticles discussed were observed, as well. The average sizes of LnF_3@SiO_2@NH_2 (Figure 3C) and LnF_3@SiO_2@NH_2@4-ethoxybenzoic acid (Figure 3D) were similar for both nanomaterials, namely approximately 50−80 nm. Their larger size in comparison to sample B was related to the higher total amount of silanes in the reaction system, and probably to a sparser silica structure, caused by the presence of amine groups. Organic modification did not influence the nanoparticles size observed in the TEM images (similar size/shape for both C and D samples). The nanoparticles obtained revealed relatively narrow size/shape distributions. TEM measurements of the core/shell type nanostructures did not reveal bare silica particles (core-free silica).

Zeta-potential measurements of the nanoparticles synthesized were carried out on their diluted aqueous colloids at adjusted pH ranging from 2 to 13. The results are presented in Figure 4. Here we must consider approximate values due to the uncertainties of the values measured (represented by the depicted error bars). Also, the measurements were performed for discrete values of the pH. Core nanoparticles (LnF_3) exhibited a positive ζ-potential of around +35 mV in a wide pH range (from 2 to 9). There was a sudden drop of the ζ-potential which appeared upon changing the pH from 9 to 10. The isoelectric point (Ip), i.e., the pH at which the value of the ζ-potential equals 0, was around pH 10. The high ζ-potential values are typical for REF_3, which allows them to create stable colloidal systems. The reported literature value of Ip for bare (ligand free) REF_3 was estimated to be around pH ≈ 6.[44] In our case the difference from the literature data was probably caused by the presence of glycerine molecules attached to the nanoparticles' surface during the synthesis. Because of this fact, their aqueous colloids were very stable in a wide pH range (2−9). LnF_3/SiO_2 nanostructures had positive ζ-potential in the pH range from 2 to 3, which decreased to around −20 mV at pH = 5. The Ip was at pH = 4. It is well-known that the isoelectric point of amorphous silica is around pH 2−4 and its pK_a ≈ 7.[45,46] That was why below pH 4 the measured ζ-potential was positive (protonated $-SiOH_2^+$ surface moieties), decreased to −20 mV at pH around 5, and then dropped to −30 mV above pH 7 (deprotonated $-SiO^-$). LnF_3@SiO_2@NH_2 nanoparticles exhibited a change of ζ-potential from +45 to −20 mV when pH was changed from 4 to 7. Two steps were observed. First we noticed a decrease to around 0 mV above pH = 4, which was probably connected with unbounded silicon groups. The second drop (to −20 mV) above pH 6 was related to amine deprotonation and the formation of neutral amino groups ($-NH_3^+ \rightarrow -NH_2$) as well as further silica deprotonation. The determined Ip was around pH 6, which undoubtedly confirmed the silica surface modification. It is in good agreement with literature data for amine modified silica particles.[33,47] LnF_3@SiO_2@NH_2@4-ethoxybenzoic acid nano-

dx.doi.org/10.1021/la501107a | Langmuir 2014, 30, 9533−9543

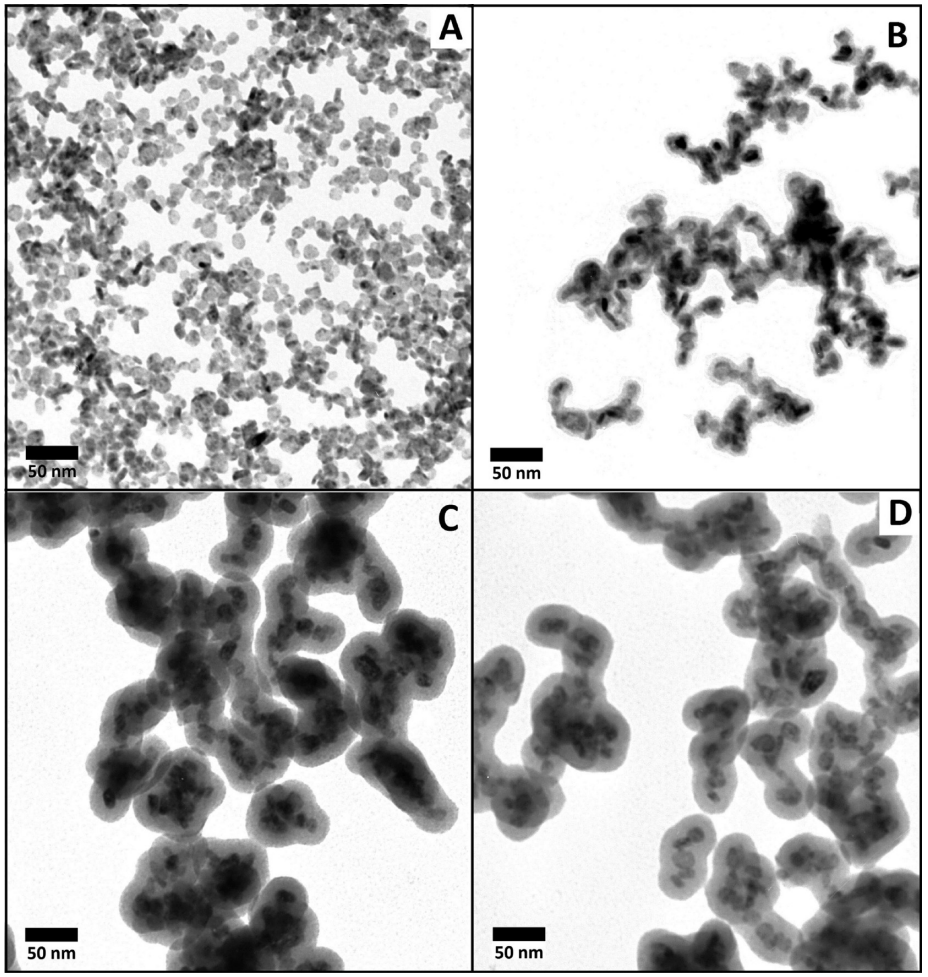

Figure 3. TEM images of CeF_3:Tb^{3+} 5%, Gd^{3+} 5% (A), CeF_3:Tb^{3+} 5%, Gd^{3+} 5%@SiO_2 (B), CeF_3:Tb^{3+} 5%, Gd^{3+} 5%@SiO_2@NH_2 (C), and CeF_3:Tb^{3+} 5%, Gd^{3+} 5%@SiO_2@NH_2@4-ethoxybenzoic acid (D) nanomaterials.

structure exhibited an isoelectric point (Ip) at around pH 4.5. No two step change was observed. The decreased Ip in comparison to the amine modified core/shell nanoparticles was due to the surface binding between amino groups and 4-ethoxybenzoic acid. In acidic and basic conditions the organic molecules were probably released. In range of low and high pH the value of the ζ-potentials of samples C and D were almost identical. Two peaks of the ζ-potential were visible at pH = 4 and 11. This was probably due to nonideal saturation of amino groups with organic molecules at values of the pH close to the release points.

The behavior of nanostructures in the pH range changing from 5 to 7 is interesting due to possible bioapplications. For such values of the pH, the high positive ζ-potential for the core nanoparticles became negative after silica coating. The amine modified silica exhibited much a higher ζ-potential then the nonmodified silica. After surface modification with 4-ethoxybenzoic acid, the ζ-potential became more negative comparedto the nonconjugated LnF_3@SiO_2@NH_2 nanostructures. Generally, all of the samples were stable at this pH range due to nonzero ζ-potentials. Changing the nature of the surface might be of interest for different bioimaging assays. The recorded size distribution histograms of the obtained nanomaterials are presented and discussed in the Supporting Information (Figure S1).

The recorded FT-IR spectra of all synthesized nanomaterials as well as their detailed interpretation are presented in the Supporting Information (Figures S2 and S3). The spectra revealed the presence of silica, amino groups, and 4-ethoxybenzoic acid in the nanomaterials obtained, confirming the desired surface modification of the nanoparticles.

In order to determine the amount of organic acid and amino groups in the nanomaterials obtained, elemental analyses of LnF_3@SiO_2@NH_2 and LnF_3@SiO_2@NH_2@4-ethoxybenzoic acid were performed. For the amine modified sample C, the obtained content of N, C, and H was 1.011, 2.737, and 1.550 wt %, respectively, whereas for sample D, modified with organic acid, the values were 0.740, 6.464, and 1.680 wt %, respectively. On the basis of the values obtained, the molar concentrations of the amino groups for the sample C (0.722 mmol/g) and 4-ethoxybenzoic acid molecules for sample D (0.345 mmol/g) were determined. The results obtained proved the high concentration of surface functional groups, confirming a successful nanomaterials functionalization, and revealed that approximately half of the amino groups were conjugated with the organic acid molecules.

4.2. Luminescent Properties. In Figures 5a–c spectroscopic properties of the nanomaterials synthesized are presented. All of the measurements were performed in the solid state (dried powders). The luminescent phase of the nanomaterials synthesized was composed of the crystalline

dx.doi.org/10.1021/la501107a | *Langmuir* 2014, 30, 9533–9543

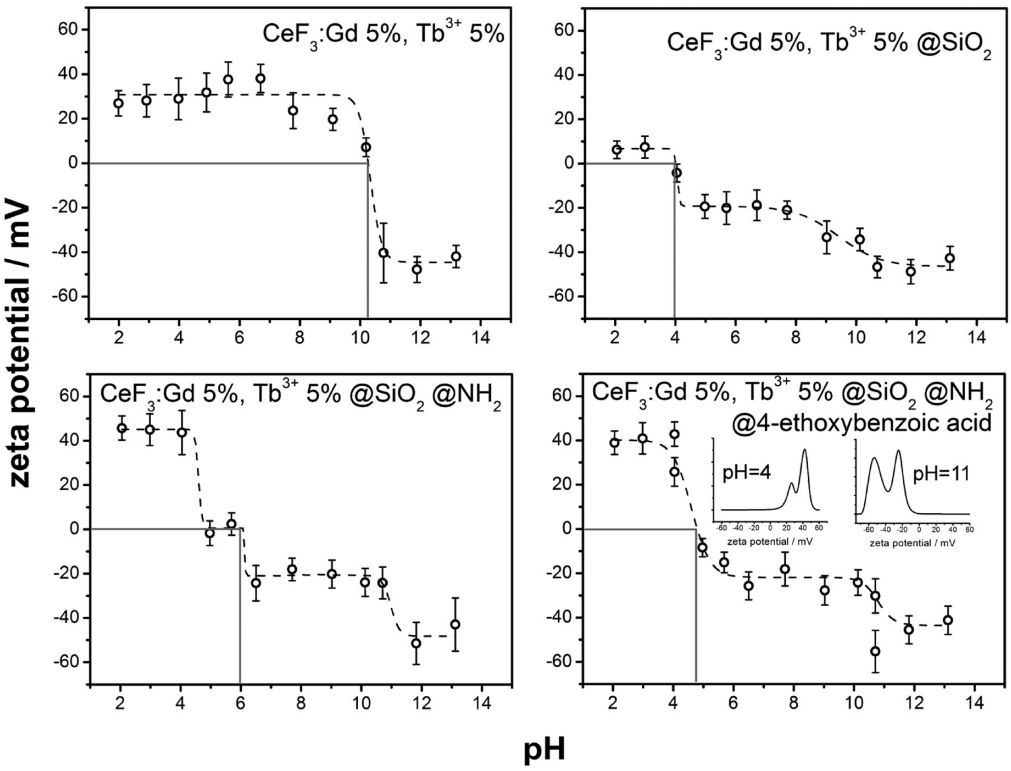

Figure 4. ζ-potential titration plots of CeF_3:Tb^{3+} 5%, Gd^{3+} 5%, CeF_3:Tb^{3+} 5%, Gd^{3+} 5%@SiO_2, CeF_3:Tb^{3+} 5%, Gd^{3+} 5%@SiO_2@NH_2 and CeF_3:Tb^{3+} 5%, Gd^{3+} 5%@SiO_2@NH_2@4-ethoxybenzoic acid diluted aqueous colloids.

CeF_3:Tb^{3+} 5%, Gd^{3+} 5% exhibiting ET phenomenon, in order to get the intense green emission of the Tb^{3+} ions. Direct Tb^{3+} excitation does not provide efficient luminescence because of the forbidden character of the 4f−4f transitions within Tb^{3+} ions.[11] In this system Ce^{3+} ions acted as energy donors, Tb^{3+} as energy acceptors (luminescence activators), and Gd^{3+} facilitated the ET from Ce^{3+} to Tb^{3+} ions, decreasing the energy gap between their lowest excited states.[14] The amount of dopants was fixed at 5% to provide efficient luminescence of the nanomaterials synthesized (due to energy transfer from Ce^{3+} and Gd^{3+} do Tb^{3+} ions) as well as to limit concentration quenching of Tb^{3+} ions and the amount of the precious Ln^{3+} ions used.[48] The concentration quenching phenomenon is commonly observed in the case of Ln^{3+}-doped materials and results in luminescence decrease and lifetime shortening.[2,11,48]

Figure 5a represents the normalized excitation spectra of the four products, recorded at λ_{em} = 543 nm (the highest emission band of Tb^{3+}). All spectra exhibited a very intense and broad absorption band around 250 nm, corresponding to the allowed $4f^1 \rightarrow 4f^05d^1$ transition in the Ce^{3+} ions (excitation of the Ce^{3+} ions), causing efficient ET to the Tb^{3+} ions.[11] Also, low-intensity absorption bands at lower energy related to the forbidden 4f → 4f transitions in the Tb^{3+} ions were observed. The core/shell type compounds obtained, having a silica shell in their structure, revealed slight shifts of the ET band and altered shapes in comparison to the pure core nanoparticles. This was because of the light absorption/scattering by the silica shell.[23,43] Also, the nanomaterial modified with 4-ethoxybenzoic acid exhibited a changed shape of the mentioned band due to UV light absorption by the organic acid in this region.

The emission spectra of the nanostructures were recorded under excitation at λ_{ex} =247 nm, in the range of the most intense ET band (Figure 5b). The products exhibited four narrow bands, characteristic of the Tb^{3+} ions, namely, $^5D_4 \rightarrow {}^7F_6$, $^5D_4 \rightarrow {}^7F_5$, $^5D_4 \rightarrow {}^7F_4$, and $^5D_4 \rightarrow {}^7F_3$ transitions corresponding to the magnetic dipole transitions in the 4f shell of the Tb^{3+} ions. When the concentration of the Tb^{3+} ions is low (usually much below 1%), a blue emission from the $^5D_3$ manifold can occur, if an appropriately remote distance between neighboring Tb^{3+} ions is preserved.[49] In our case emission bands connected with transitions from this level were not observed. All emission spectra had the same shape because of the similar chemical environment around Tb^{3+} ions. Such transitions are generally not sensitive to the coordination environment symmetry of the emitting ions.[11,26] Nanoparticles of the bare core exhibited the highest emission intensities, which can be clearly seen in the discussed spectra (red curve). The three products bearing silica shells exhibited similar intensity to each other, however significantly lower in comparison to the core nanoparticles (without silica). This was caused by light absorption/scattering by the silica shells.[43] Among these compounds, the one having a nonmodified silica shell (CeF_3:Tb^{3+}, Gd^{3+}@SiO_2) revealed the smallest emission intensity. The efficient luminescence quenching by O−H oscillators from water molecules was a reason for this behavior. In the spectrum of the product modified with 4-ethoxybenzoic acid, an intense broad emission band centered at 400 nm was observed (green curve). This band was assigned to the luminescence of the 4-ethoxybenzoic acid, attached to the nanoparticles' surface. It was an additional confirmation of the successful organic modification of our nanomaterial. In the Supporting Information (Figure S4) the excitation and emission spectra of the pure 4-ethoxybenzoic acid are shown. The discussed organic acid attached to the surface of nanoparticles exhibited a bathochromic shift in comparison to

dx.doi.org/10.1021/la501107a | Langmuir 2014, 30, 9533−9543

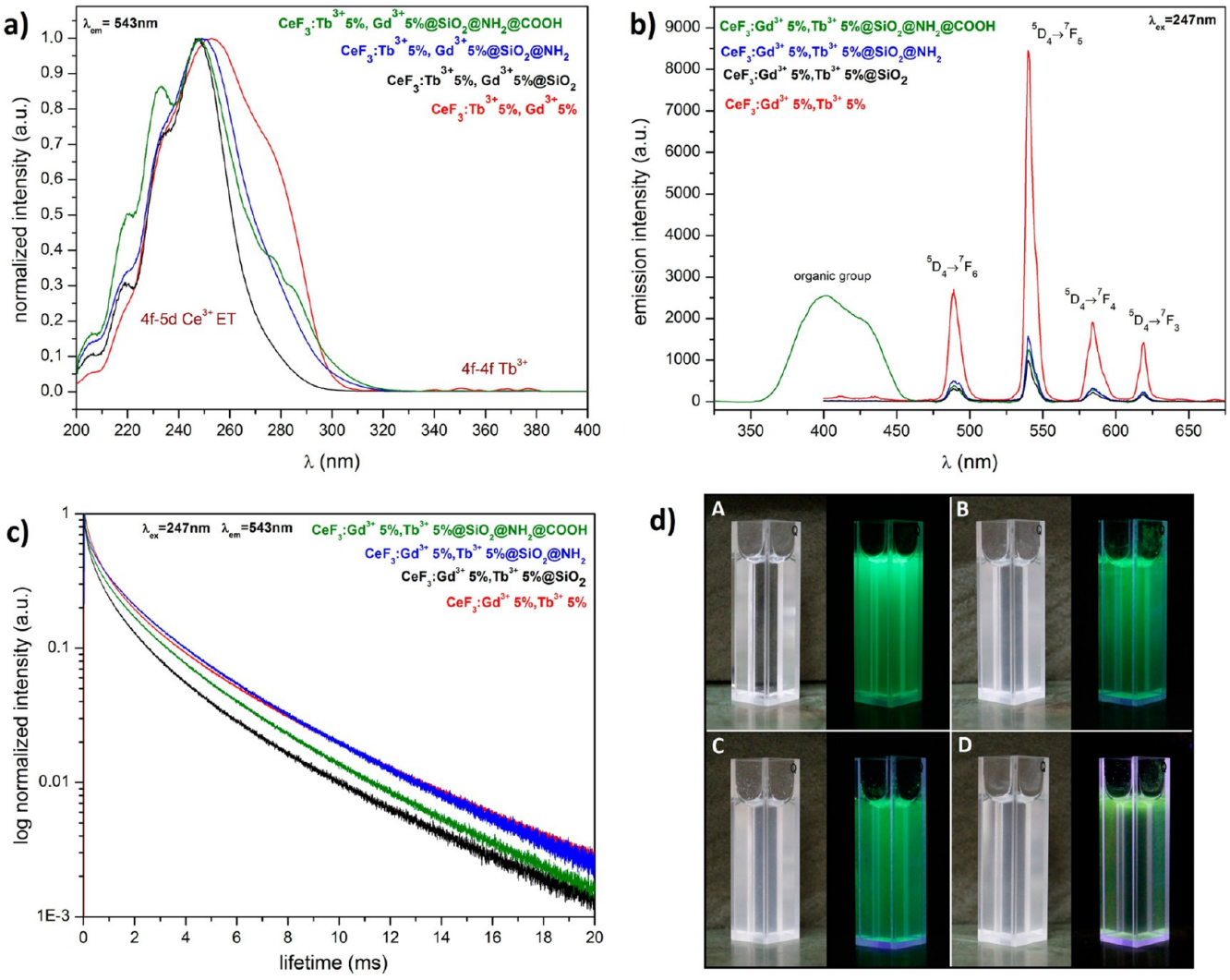

Figure 5. Excitation (a), emission spectra (b), and luminescence decay curves (c) of CeF_3:Tb^{3+} 5%, Gd^{3+} 5%, CeF_3:Tb^{3+} 5%, Gd^{3+} 5%@SiO_2, CeF_3:Tb^{3+} 5%, Gd^{3+} 5%@SiO_2@NH_2 and CeF_3:Tb^{3+} 5%, Gd^{3+} 5%@SiO_2@NH_2@4-ethoxybenzoic acid, recorded at λ_{em} = 543 nm and λ_{ex} = 247 nm. Photographs (d) of the obtained aqueous colloids of CeF_3:Tb^{3+} 5%, Gd^{3+} 5% (A), CeF_3:Tb^{3+} 5%, Gd^{3+} 5%@SiO_2 (B), CeF_3:Tb^{3+} 5%, Gd^{3+} 5% @SiO_2@NH_2 (C), and CeF_3:Tb^{3+} 5%, Gd^{3+} 5%@SiO_2@NH_2@4-ethoxybenzoic acid (D) nanomaterials, taken in a daylight (left) and under UV (254 nm) lamp irradiation (right).

the free acid because of the alternations of its coordination environment.

The measured luminescence decay curves depicted in Figure 5c showed nonexponential character, because of the quenching processes of the Tb^{3+} ions embedded in the crystalline structures. However, in order to compare the luminescence lifetimes of the nanomaterials synthesized, the recorded decay profiles were fitted to a mathematical function representing biexponential character ($R > 0.99$), namely, $y = A_1 \exp(-x/t_1) + A_2 \exp(-x/t_2) + y_0$. The bulk CeF_3 should reveal only one site symmetry for all Ln^{3+} ions, resulting in monoexponential luminescence decay. Therefore, we assumed that the second short-lived lifetime component corresponded to the surface and near surface ions because of a high quenching probability of such Tb^{3+} ions. The calculated lifetime values are presented in Table 1. In all samples the short-lived components were dominant. This proved there was a significant contribution of surface ions to the total luminescence of the products and also the relatively high surface to volume ratio of the NPs. The shortest average lifetime was observed in the nanomaterial modified with the organic acid, which confirmed the quenching

Table 1. Calculated Radiative Lifetimes Values (τ_1 and τ_2) of the Nanophosphors Obtained

compound	τ_1 (ms)	τ_2 (ms)
LnF_3 (CeF_3:Tb^{3+} 5%, Gd^{3+} 5%)	3.48 (31%)	0.59 (69%)
LnF_3@SiO_2	3.05 (28%)	0.55 (72%)
LnF_3@SiO_2@NH_2	3.43 (40%)	0.67 (60%)
LnF_3@SiO_2@NH_2@4-ethoxybenzoic acid	3.18 (32%)	0.49 (68%)

influence of the organic compound on Tb^{3+} emission. The longest emission lifetimes were recorded for the bare core and the amine modified core/shell type product. The observed increase of the lifetime for LnF_3@SiO_2@NH_2 nanomaterial in comparison to the LnF_3@SiO_2 was probably caused by the protecting role of the amino groups against the quenching influence of water molecules. The relatively long lifetimes obtained for the nanomaterials synthesized are in good agreement with data reported in the literature for Tb^{3+}-doped inorganic systems.[11,13]

The photographs of the aqueous colloidal solutions of the nanomaterials obtained are presented in Figure 5d, namely,

dx.doi.org/10.1021/la501107a | Langmuir 2014, 30, 9533−9543

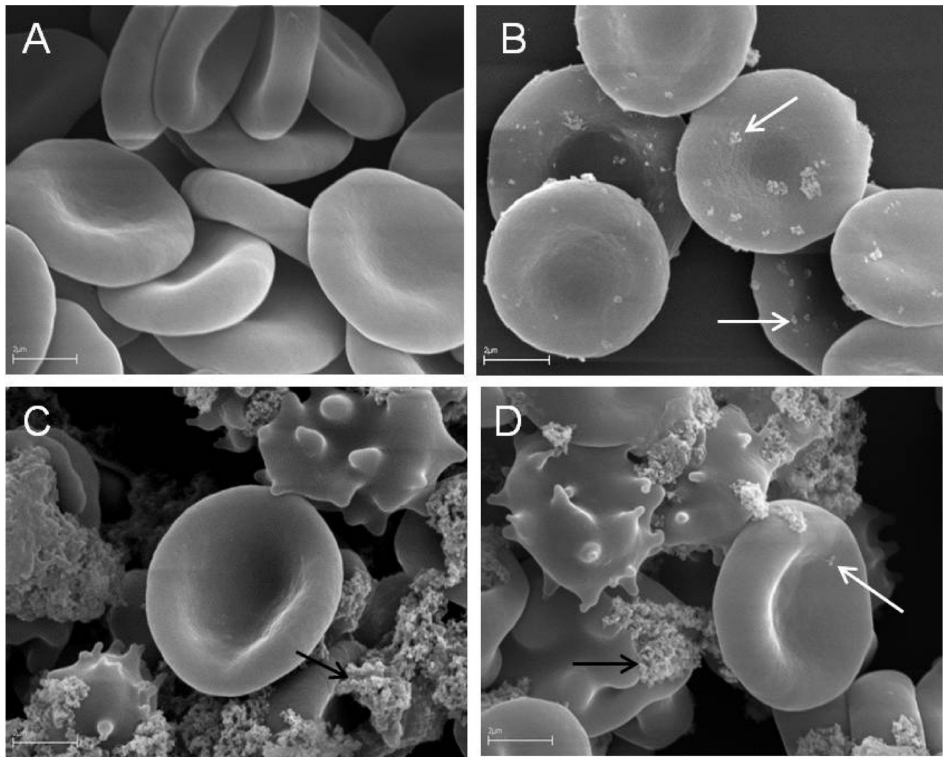

Figure 6. Effect of (A) PBS (control), (B) CeF_3:Tb^{3+} 5%, Gd^{3+} 5%, (C) CeF_3:Tb^{3+} 5%, Gd^{3+} 5%@SiO_2@NH_2, and (D) CeF_3:Tb^{3+} 5%, Gd^{3+} 5%@SiO_2@NH_2@4-ethoxybenzoic acid at the concentration 1 mg/mL, on human erythrocytes morphology as observed by scanning electron microscope. White arrows: single particles; black arrows: particles aggregates. Scale bars indicate 2 μm. CeF_3:Tb^{3+} 5%, Gd^{3+} 5%@SiO_2 treated cells are not shown because of 100% hemolysis.

LnF_3 (A), LnF_3@SiO_2 (B), LnF_3@SiO_2@NH_2 (C), and LnF_3@SiO_2/NH_2/4-ethoxybenzoic acid (D). Each colloid was prepared by dispersing the given nanomaterial in water, with the use of ultrasound, at a fixed concentration of the solid phase, equal to 0.5 mg/mL. The pictures of the colloids prepared were taken in daylight (left) and under a UV (254 nm) lamp irradiation (right), revealing their bright green luminescence. All of the colloids obtained were stable over many days. The colloid containing pure cores showed the most intense emission. Modification of the cores (surface coating) decreased the total amount of the luminescent phase in the final products, which is the direct reason for the lowered luminescence intensity observed in Figure 5d (photos B–D).

4.3. Cytotoxicity Properties of the Nanoparticles. The cytotoxicity properties of the nanoparticles synthesized were studied using human erythrocytes as a simple cell model. The CeF_3: Tb^{3+}, Gd^{3+} (LnF_3) nanomaterials were bound to the erythrocyte membrane as single particles or as small particle aggregates. However, it did not induce cell shape alterations (Figure 6B, compare with Figure 6A—control cells, dysco-cytes) and did not increase membrane permeability and hemolysis, in the concentrations tested. The erythrocytes under the bare core treatment settled with a different rate as compared with the control erythrocytes (Figure S5), at the concentrations of 1 and 0.1 mg/mL. No influence of LnF_3 nanocrystals at the concentration of 0.01 mg/mL on the erythrocyte sedimentation rate was observed. Our data confirm the results presented in other studies, where rare-earth-based nanoparticles had no or only a small effect on mammalian cells tested *in vitro*, both cancer and normal ones.[23,50,51] However, different lanthanide-doped nanocrystals, like cerium oxide, demonstrated toxic properties, especially for cancer cells.[52,53]

In contrast, the analysis of LnF_3 encapsulated in silica shells revealed significant toxicity properties toward human erythrocytes (100% hemolysis), at concentrations of 1 and 0.1 mg/mL, and less cytotoxicity (more than 10% hemolysis) at the concentration of 0.01 mg/mL (Figure S5). The negative effect of LnF_3@SiO_2 on the erythrocyte membrane structure (hemolysis) and the sedimentation rate disappeared at a concentration of 0.001 mg/mL. The results of this study are in agreement with other data showing substantial cytotoxicity of nanomaterials containing SiO_2.[27,28] In those earlier investigations, the toxicity effects were also in a dose-dependent manner; however, the cells (such as human lung cancer cells, HaCaT cells, bone marrow mesenchymal stem cells, or skeletal myoblasts) were treated with NPs at a concentration higher than 0.001 mg/mL (the concentration which was nontoxic for the erythrocytes in our study). Here it is worth noting that according to the other research,[32,54] silica can exert negligible cytotoxic effects toward erythrocytes, dependent on the size of the silica particles and their surface properties mostly.

Both LnF_3@SiO_2@NH_2 and LnF_3@SiO_2@NH_2@4-ethoxybenzoic acid induced shape alterations (echinocytosis) and hemolysis ($\geq$ 10%) in the erythrocytes at the concentration of 1 mg/mL. Large self-aggregates of NPs bound to the erythrocytes induced their echinocytic transformations (Figure 6C,D). At NPs concentrations of 0.1 and 0.01 mg/mL, there was no cell hemolysis observed, and the erythrocyte's sedimentation rate was not affected (Figure S5). These outcomes confirmed previous investigations which demonstrated that functionalization of silica-coated nanoparticles with amino or carboxyl groups can reduce their cytotoxicity properties.[55] Amino groups may protect cells from interactions with surface silane. However, other studies indicated that

dx.doi.org/10.1021/la501107a | *Langmuir* 2014, 30, 9533–9543

functionalization of silica nanoparticles with amino groups may increase their cytotoxic properties, depending of their surface structure and charge.[32,39]

In summary, the CeF_3:Tb^{3+} 5%, Gd^{3+} 5% nanoparticles could bind to red blood cell membranes as single particles without any cell shape transformation (Figure 6B), and they did not induce any changes in the structure of the membranes of the erythrocytes. The NPs binding to the erythrocytes occurred probably by interactions of the positive bare core with the negatively charged cell membrane. In contrast, NPs coated with silica revealed substantial cytotoxic properties, whereas the nanoparticles having silica functionalized with $-NH_2$ groups as well as with 4-ethoxybenzoic acid formed self-aggregates in the solution and revealed weak hemolytic activity. These aggregates bound to the erythrocytes surface inducing their echinocytic transformation (Figure 6C,D). The similar results to our were obtained by Zhao et al., in the case of 100−200 nm size mesoporous silica nanoparticles.[40] A silanol-rich surface of the silica was bound to the phosphatidylcholine-rich erythrocytes' membrane.

5. CONCLUSIONS

The luminescent CeF_3:Tb^{3+} 5%, Gd^{3+} 5% (LnF_3 core), LnF_3@SiO_2, and LnF_3@SiO_2@NH_2 (core/shell) nanoparticles were successfully synthesized and surface modified via facile, low-cost, and easy to scale-up methods. The nanostructures obtained were composed of nanocrystalline LnF_3 cores exhibiting intense green luminescence under UV light irradiation. The cores synthesized were coated with an external amine modified silica shell. Subsequently, the nanostructures obtained were successfully functionalized with 4-ethoxybenzoic acid, as an exemplary reactive and functional organic compound, which can be used for surface modifications. The formation of core/shell type nanoparticles, their structure, and surface modification with amino groups and carboxylic acid molecules were confirmed by XRD, TEM, and DLS measurements. On the basis of the performed ζ-potential titrations, the isoelectric points (Ip) of all of the obtained nanomaterials were determined. All synthesized nanomaterials formed stable aqueous colloids exhibiting green luminescence under UV lamp irradiation (λ_{ex} = 254 nm). The cytotoxicity assays revealed that all of the prepared nanomaterials can interact with human erythrocyte membranes. Silica coating and functionalization of the nanoparticles with $-NH_2$ groups as well as conjugation with 4-ethoxybenzoic acid induced significant changes of erythrocyte membrane perturbing properties, resulting in altered cytotoxic properties. These findings may be useful in the process of creating new NPs safe for living cells and for subsequent studies conducted on biomolecule delivery, e.g., in the organism. The results obtained can increase the impact of inorganic, lanthanide doped nanophosphors on fundamental biomedical research, as biomarkers, contrast agents, drug-delivery systems, etc.

■ ASSOCIATED CONTENT

Supporting Information

Preparation of 4-ethoxybenzoyl chloride; characterization of cytotoxicity assays; hydrodynamic diameters plots of CeF_3:Tb^{3+} 5%, Gd^{3+} 5%, CeF_3:Tb^{3+} 5%, Gd^{3+} 5%@SiO_2, CeF_3:Tb^{3+} 5%, Gd^{3+} 5%@SiO_2@NH_2, and CeF_3:Tb^{3+} 5%, Gd^{3+} 5%@SiO_2@NH_2@4-ethoxybenzoic acid, recorded at different pH values (2−13), and the insets presenting grain size distribution histograms for each compound, recorded at pH = 7 (Figure S1); FT-IR spectra of the nanomaterials synthesized (Figure S2) and spectra comparison of CeF_3:Tb^{3+} 5%, Gd^{3+} 5%@SiO_2@NH_2@4-ethoxybenzoic acid nanomaterial, before (a) and after (b) organic acid release from the surface at acidic pH (Figure S3); excitation (dotted line) and emission (continuous line) spectra of pure 4-ethoxybenzoic acid, recorded at λ_{em} = 335 nm and λ_{ex} = 247 nm, respectively (Figure S4); effect of the nanoparticles synthesized on the erythrocyte sedimentation rate (Figure S5). This material is available free of charge via the Internet at http://pubs.acs.org.

■ AUTHOR INFORMATION

Corresponding Authors

*E-mail blis@amu.edu.pl (S.L.).
*E-mail anna.ekner@gmail.com (A.E.G.).

Notes

The authors declare no competing financial interest.

■ ACKNOWLEDGMENTS

S.L., A.E.G., and T.G. kindly acknowledge the financial support from the National Science Centre (Grant DEC-2012/06/M/ST5/00325). M.R. gratefully acknowledges the financial support from Polish Ministry of Science and Higher Education—scientific work was financed from the budget for science in 2012−2015 as a research project within the program called "Diamond Grant" Nr DI2011 011441. J.P.'s work was supported by the National Science Centre within SONATA grant according to decision number DEC-2012/07/D/ST5/02240. A.Z. gratefully acknowledges the financial support from FNP Project TEAM/2010-5/4, "Self-assembly of functionalized inorganic−organic liquid crystalline hybrids for multifunctional nanomaterials". T.G. holds a scholarship from the Foundation for Polish Science for Young Scientists (FNP).

■ REFERENCES

(1) Selvan, S. T.; Tan, T. T. Y.; Yi, D. K.; Jana, N. R. Functional and Multifunctional Nanoparticles for Bioimaging and Biosensing. *Langmuir* **2009**, *26*, 11631−11641.

(2) Runowski, M.; Lis, S. Preparation and Photophysical Properties of Luminescent Nanoparticles Based on Lanthanide Doped Fluorides (LaF_3:Ce^{3+}, Gd^{3+}, Eu^{3+}), Obtained in the Presence of Different Surfactants. *J. Alloys Compd.* **2014**, *597*, 63−71.

(3) Xing, Y.; Chaudry, Q.; Shen, C.; Kong, K. Y.; Zhau, H. E.; Chung, L. W.; Petros, J. A.; O'Regan, R. M.; Yezhelyev, M. V.; Simons, J. W.; Wang, M. D.; Nie, S. Bioconjugated Quantum Dots for Multiplexed and Quantitative Immunohistochemistry. *Nat. Protoc.* **2007**, *2*, 1152−1165.

(4) Skumryev, V.; Stoyanov, S.; Zhang, Y.; Hadjipanayis, G.; Givord, D.; Nogués, J. Beating the Superparamagnetic Limit with Exchange Bias. *Nature* **2003**, *423*, 850−853.

(5) Yu, J. C.; Yu, J.; Zhang, L.; Ho, W. Enhancing Effects of Water Content and Ultrasonic Irradiation on the Photocatalytic Activity of Nano-sized TiO_2 Powders. *J. Photochem. Photobiol. A: Chem.* **2002**, *148*, 263−271.

(6) Bünzli, J.-C. G.; Eliseeva, S. V. Lanthanide NIR Luminescence for Telecommunications, Bioanalyses and Solar Energy Conversion. *J. Rare Earths* **2010**, *28*, 824−842.

(7) Eliseeva, S. V.; Bünzli, J.-C. G. Rare Earths: Jewels for Functional Materials of the Future. *New J. Chem.* **2011**, *35*, 1165−1176.

(8) Kang, X.; Yang, D.; Ma, P.; Dai, Y.; Shang, M.; Geng, D.; Cheng, Z.; Lin, J. Fabrication of Hollow and Porous Structured $GdVO_4$:Dy^{3+} Nanospheres as Anticancer Drug Carrier and MRI Contrast Agent. *Langmuir* **2013**, *29*, 1286−1294.

(9) Gagné, F.; Maysinger, D.; André, C.; Blaise, C. Cytotoxicity of Aged Cadmium-telluride Quantum Dots to Rainbow Trout Hepatocytes. *Nanotoxicology* **2008**, *2*, 113−120.
(10) Grzyb, T.; Gruszeczka, A.; Wiglusz, R. J.; Lis, S. The Effects of Down- and Up-conversion on Dual-Mode Green Luminescence from Yb^{3+}- and Tb^{3+}-Doped $LaPO_4$ Nanocrystals. *J. Mater. Chem. C* **2013**, *1*, 5410−5418.
(11) Grzyb, T.; Runowski, M.; Szczeszak, A.; Lis, S. Influence of Matrix on the Luminescent and Structural Properties of Glycerine-Capped, Tb^{3+}-Doped Fluoride Nanocrystals. *J. Phys. Chem. C* **2012**, *116*, 17188−17196.
(12) Kömpe, K.; Borchert, H.; Storz, J.; Lobo, A.; Adam, S.; Möller, T.; Haase, M. Green-Emitting $CePO_4$:Tb/$LaPO_4$ Core-Shell Nanoparticles with 70% Photoluminescence Quantum Yield. *Angew. Chem., Int. Ed.* **2003**, *42*, 5513−5516.
(13) Li, C.; Liu, X.; Yang, P.; Zhang, C.; Lian, H.; Lin, J. LaF_3, CeF_3, CeF_3:Tb^{3+}, and CeF_3:Tb^{3+}@LaF_3 (Core-Shell) Nanoplates: Hydrothermal Synthesis and Luminescence Properties. *J. Phys. Chem. C* **2008**, *112*, 2904−2910.
(14) Wang, F.; Fan, X.; Wang, M.; Zhang, Y. Multicolour PEI/$NaGdF_4$:Ce^{3+},Ln^{3+} Nanocrystals by Single-Wavelength Excitation. *Nanotechnology* **2007**, *18*, 25701−25706.
(15) Weber, M. J. Probabilities for Radiative and Nonradiative Decay of Er^{3+} in LaF_3. *Phys. Rev.* **1967**, *157*, 262−272.
(16) Zhang, Q.; Wang, X.; Zhu, Y. Multicolor Upconverted Luminescence-encoded Superparticles via Controlling Self-assembly Based on Hydrophobic Lanthanide-Doped $NaYF_4$ Nanocrystals. *J. Mater. Chem.* **2011**, *21*, 12132−12138.
(17) Stouwdam, J. W.; Hebbink, G. A.; Huskens, J.; van Veggel, F. C. J. M. Lanthanide-Doped Nanoparticles with Excellent Luminescent Properties in Organic Media. *Chem. Mater.* **2003**, *15*, 4604−4616.
(18) Lemyre, J.-L.; Ritcey, A. M. Synthesis of Lanthanide Fluoride Nanoparticles of Varying Shape and Size. *Chem. Mater.* **2005**, *17*, 3040−3043.
(19) Boulon, G. Fifty Years of Advances in Solid-state Laser Materials. *Opt. Mater.* **2012**, *34*, 499−512.
(20) Yang, P.; Quan, Z.; Hou, Z.; Li, C.; Kang, X.; Cheng, Z.; Lin, J. A Magnetic, Luminescent and Mesoporous Core-Shell Structured Composite Material as Drug Carrier. *Biomaterials* **2009**, *30*, 4786−4795.
(21) Runowski, M.; Grzyb, T.; Lis, S. Magnetic and Luminescent Hybrid Nanomaterial Based on Fe_3O_4 Nanocrystals and $GdPO_4$:Eu^{3+} Nanoneedles. *J. Nanopart. Res.* **2012**, *14*, 1188−1195.
(22) Joo, S. H.; Park, J. Y.; Tsung, C.-K.; Yamada, Y.; Yang, P.; Somorjai, G. A. Thermally Stable Pt/Mesoporous Silica Core-Shell Nanocatalysts for High-Temperature Reactions. *Nat. Mater.* **2009**, *8*, 126−131.
(23) Grzyb, T.; Runowski, M.; Dąbrowska, K.; Giersig, M.; Lis, S. Structural, Spectroscopic and Cytotoxicity Studies of TbF_3@CeF_3 and TbF_3@CeF_3@SiO_2 Nanocrystals. *J. Nanopart. Res.* **2013**, *15*, 1958−1972.
(24) Mahon, E.; Hristov, D. R.; Dawson, K. A. Stabilising Fluorescent Silica Nanoparticlesagainst Dissolution Effects for Biological Studies. *Chem. Commun.* **2012**, *48*, 7970−7972.
(25) Jana, N. R.; Earhart, C.; Ying, J. Y. Synthesis of Water-Soluble and Functionalized Nanoparticles by Silica Coating. *Chem. Mater.* **2007**, *19*, 5074−5082.
(26) Runowski, M.; Dąbrowska, K.; Grzyb, T.; Miernikiewicz, P.; Lis, S. Core/Shell-Type Nanorods of Tb^{3+}-Doped $LaPO_4$, Modified with Amine Groups, Revealing Reduced Cytotoxicity. *J. Nanopart. Res.* **2013**, *15*, 2068−2083.
(27) Lin, W.; Huang, Y.-W.; Zhou, X.-D.; Ma, Y. In Vitro Toxicity of Silica Nanoparticles in Human Lung Cancer Cells. *Toxicol. Appl. Pharmacol.* **2006**, *217*, 252−259.
(28) Yang, X.; Liu, J.; He, H.; Zhou, L.; Gong, C.; Wang, X.; Yang, L.; Yuan, J.; Huang, H.; He, L.; Zhang, B.; Zhuang, Z. SiO_2 Nanoparticles Induce Cytotoxicity and Protein Expression Alteration in HaCaT Cells. *Part. Fibre Toxicol.* **2010**, *7*, 1−12.
(29) Corbalan, J. J.; Medina, C.; Jacoby, A.; Malinski, T.; Radomski, M. W. Amorphous Silica Nanoparticles Aggregate Human Platelets: Potential Implications for Vascular Homeostasis. *Int. J. Nanomedicine* **2012**, *7*, 631−639.
(30) Yu, T.; Malugin, A.; Ghandehari, H. Impact of Silica Nanoparticle Design on Cellular Toxicity and Hemolytic Activity. *ACS Nano* **2011**, *5*, 5717−5728.
(31) Napierska, D.; Thomassen, L. C. J.; Rabolli, V.; Lison, D.; Gonzalez, L.; Kirsch-Volders, M.; Martens, J. A.; Hoet, P. H. Size-dependent cytotoxicity of monodisperse silica nanoparticles in human endothelial cells. *Small* **2009**, *5*, 836−853.
(32) Yu, T.; Malugin, A.; Ghandehari, H. Impact of Silica Nanoparticle Design on Cellular Toxicity and Hemolytic Activity. *ACS Nano* **2011**, *5*, 5717−5728.
(33) Wang, J.; Zheng, S.; Shao, Y.; Liu, J.; Xu, Z.; Zhu, D. Amino-Functionalized Fe_3O_4@SiO_2 Core-Shell Magnetic Nanomaterial as a Novel Adsorbent for Aqueous Heavy Metals Removal. *J. Colloid Interface Sci.* **2010**, *349*, 293−299.
(34) Fröhlich, E. Europe PMC Funders Group Cellular Targets and Mechanisms in the Cytotoxic Action of Non- Biodegradable Engineered Nanoparticles. *Curr. Drug Metab.* **2013**, *14*, 976−988.
(35) Stoccoro, A.; Karlsson, H. L.; Coppedè, F.; Migliore, L. Epigenetic Effects of Nano-sized Materials. *Toxicology* **2013**, *313*, 3−14.
(36) Monopoli, M. P.; Åberg, C.; Salvati, A.; Kenneth, A.; Dawson, K. A. Biomolecular Coronas Provide the Biological Identity of Nanosized Materials. *Nat. Nanotechnol.* **2012**, *7*, 779−786.
(37) Park, M. V. D. Z.; Neigh, A. M.; Vermeulen, J. P.; de la Fonteyne, L. J. J.; Verharen, H. W.; Briedé, J. J.; van Loveren, H.; de Jong, W. H. The Effect of Particle Size on the Cytotoxicity, Inflammation, Developmental Toxicity and Genotoxicity of Silver Nanoparticles. *Biomaterials* **2011**, *32*, 9810−9817.
(38) Janowski, M.; Bulte, J. W. M.; Walczak, P. Personalized Nanomedicine Advancements for Stem Cell Tracking. *Adv. Drug Delivery Rev.* **2012**, *64*, 1488−1507.
(39) Shahbazi, M.-A.; Hamidi, M.; Mäkilä, E. M.; Zhang, H.; Almeida, P. V.; Kaasalainen, M.; Salonen, J. J.; Hirvonen, J. T.; Santos, H. The Mechanisms of Surface Chemistry Effects of Mesoporous Silicon Nanoparticles on Immunotoxicity and Biocompatibility. *Biomaterials* **2013**, *34*, 7776−7789.
(40) Zhao, Y.; Sun, X.; Zhang, G.; Trewyn, B. G.; Slowing, I. I.; Lin, V. S.-Y. Interaction of Mesoporous Silica Nanoparticles with Human Red Blood Cell Membranes: Size and Surface Effects. *ACS Nano* **2011**, *5*, 1366−1375.
(41) Stöber, W. Controlled Growth of Monodisperse Silica Spheres in the Micron Size Range. *J. Colloid Interface Sci.* **1968**, *26*, 62−69.
(42) Langford, J. I.; Wilson, A. J. C. Scherrer after Sixty Years: A Survey and Some New Results in the Determination of Crystallite Size. *J. Appl. Crystallogr.* **1978**, *11*, 102−113.
(43) Runowski, M.; Grzyb, T.; Lis, S. Bifunctional Luminescent and Magnetic Core/shell Type Nanostructures Fe_3O_4@CeF_3:Tb^{3+}/SiO_2. *J. Rare Earths* **2011**, *29*, 1117−1122.
(44) Bogdan, N.; Vetrone, F.; Ozin, G. A.; Capobianco, J. A. Synthesis of Ligand-Free Colloidally Stable Water Dispersible Brightly Luminescent Lanthanide-doped Upconverting Nanoparticles. *Nano Lett.* **2011**, *11*, 835−840.
(45) Philipse, A. P.; van Bruggen, M. P. B.; Pathmamanoharan, C. Magnetic Silica Dispersions: Preparation and Stability of Surface-modified Silica Particles with a Magnetic Core. *Langmuir* **1994**, *10*, 92−99.
(46) Leung, K.; Nielsen, I. M. B.; Criscenti, L. J. Elucidating the Bimodal Acid-Base Behavior of the Water-Silica Interface from First Principles. *J. Am. Chem. Soc.* **2009**, *131*, 18358−18365.
(47) Rosenholm, J. M.; Meinander, A.; Peuhu, E.; Niemi, R.; Eriksson, J. E.; Sahlgren, C.; Lindén, M. Targeting of Porous Hybrid Silica Nanoparticles to Cancer Cells. *ACS Nano* **2009**, *3*, 197−206.
(48) Holloway, W. W., Jr.; Kestigian, M. Concentration Quenching of the Tb^{3+} Ion Fluorescence in $Y_3Al_5O_{12}$ Crystals. *Phys. Lett.* **1966**, *21*, 364−366.

(49) Ricci, P. C.; Carbonaro, C. M.; Corpino, R.; Cannas, C.; Salis, M. Optical and Structural Characterization of Terbium-Doped Y_2SiO_5 Phosphor Particles. *J. Phys. Chem. C* **2011**, *115*, 16630−16636.
(50) Chatterjee, D. K.; Rufaihah, A. J.; Zhang, Y. Upconversion Fluorescence Imaging of Cells and Small Animals Using Lanthanide Doped Nanocrystals. *Biomaterials* **2008**, *29*, 937−943.
(51) Chen, X.; Zhao, Z.; Jiang, M.; Que, D.; Shi, S.; Zheng, N. Preparation and Photodynamic Therapy Application of $NaYF_4$:Yb, Tm−$NaYF_4$:Yb, Er Multifunctional Upconverting Nanoparticles. *New J. Chem.* **2013**, *37*, 1782−1788.
(52) Wason, M. S.; Zhao, J. Cerium Oxide Nanoparticles: Potential Applications for Cancer and Other Diseases. *Am. J. Transl. Res.* **2013**, *5*, 126−131.
(53) Cheng, G.; Guo, W.; Han, L.; Chen, E.; Kong, L.; Wang, L.; Ai, W.; Song, N.; Li, H.; Chen, H. Cerium Oxide Nanoparticles Induce Cytotoxicity in Human Hepatoma SMMC-7721 Cells via Oxidative Stress and the Activation of MAPK Signaling Pathways. *Toxicol. In Vitro* **2013**, *27*, 1082−1088.
(54) Zhao, Y.; Sun, X.; Zhang, G.; Trewyn, B. G.; Slowing, I. I.; Lin, V. S.-Y. Interaction of Mesoporous Silica Nanoparticles with Human Red Blood Cell Membranes: Size and Surface Effects. *ACS Nano* **2011**, *5*, 1366−1375.
(55) Nabeshi, H.; Yoshikawa, T.; Arimori, A.; Yoshida, T.; Tochigi, S.; Hirai, T.; Akase, T.; Nagano, K.; Abe, Y.; Kamada, H.; Tsunoda, S.; Itoh, N.; Yoshioka, Y.; Tsutsumi, Y. Effect of Surface Properties of Silica Nanoparticles on Their Cytotoxicity and Cellular Distribution in Murine Macrophages. *Nanoscale Res. Lett.* **2011**, *6*, 93−98.